Multigigahertz sources and photoreceivers for lightwave networks

Pallab Bhattacharya

Department of Electrical Engineering and Computer Science
University of Michigan, Ann Arbor, MI 48109-2122

ABSTRACT

High-speed optical sources and receivers are required for efficience wavelength division multiplexed (WDM) lightwave networks. The performance of high-speed GaAs- and InP-based lasers and monolithically integrated photoreceivers, suitable for this application, are described.

Keywords: high speed lasers, photoreceivers

1. INTRODUCTION

Multimedia services, cable and antenna television (CATV), high definition television (HDTV), and computer links have permeated into every aspect of our lives and have become virtually indispensable. Large amounts of data transmission via lightwave networks have and will undoubtedly continue to benefit us by improving the way of life. The demands on a network which can accommodate the entire communication traffic in a cost effective manner have drawn considerable attention and tremendous effort has been expended on this issue. Single-mode optical fibers widely deployed in today's telecommunication networks have the potential to carry 30 Tb/s. However, it is largely underutilized by even the most dense telecommunication system (2.5 Gb/s) commercially available at the present time[1, 2]. Unlike traditional time-division-multiplexing (TDM) techniques, wavelength division multiplexing (WDM) techniques offer a cost effective utilization of the fiber bandwidth directly in the wavelength domain, rather than in the time domain. Furthermore, the wavelengths can be used to perform functions as routing and switching[3], which are attractive for realization of all-optical transparent network layers in future networks.

Efficient and high-speed transmitters and receivers are required for lightwave networks operating in the multi-gigahertz range. This paper describes the design, fabrication and operational characteristics of high-speed lasers and integrated photoreceivers that are currently in use of will be used in future WDM communication systems.

2. GaAs-BASED (λ~1μm) LASERS

We will first describe the characteristics of GaAs-based ~1μm multiquantum well MQW tunneling injection lasers. Measurements have been done as a function of temperature in a variable temperature cryostat to determine the d.c. and dynamic characteristics. The optical modulation response was typically measured with a network analyzer, high speed photoreceiver and amplifier. The measured response was corrected for the frequency response of the cables, amplifier and photoreceiver. The facets of our device are uncoated.

The light-current characteristics of a MQW TI laser under pulsed bias conditions are shown in Fig. 1(a). The threshold current at room temperature is 3 mA and the slope efficiency is 0.33 mW/mA. The transparency current density, determined from a plot of J_{th} versus inverse cavity length, is only 167 A/cm^2. The emission spectrum of the device is shown in the insert of Fig. 2. The peak of the laser emission is at 0.98μm, which confirms lasing from the MQW region.

Figure 1(b) shows the modulation frequency response of the undoped MQW tunneling injection laser at room temperature under pulsed and CW bias conditions. The maximum modulation bandwidth was achieved at a drive current of 80 mA under pulsed bias conditions. The extrapolated -3 dB modulation bandwidth is ~45 GHz. From a plot of the damping factor γ vs. f_r^2 shown in Fig. 1(c) the K-factor is 0.105 ns, representing a maximum intrinsic bandwidth, $f_{-3\ dB(max)}$ of 84 GHz. For CW operation the modulation characteristics are $f_{-3\ dB}$=43 GHz, K=0.116 ns, and $f_{-3\ dB(max)}$=76 GHz. These high-speed modulation characteristics are better than those normally achieved with conventional SCH quantum well lasers[4].

Part of the SPIE Conference on Terahertz and Gigahertz Photonics • Denver, Colorado • July 1999
SPIE Vol. 3795 • 0277-786X/99/$10.00

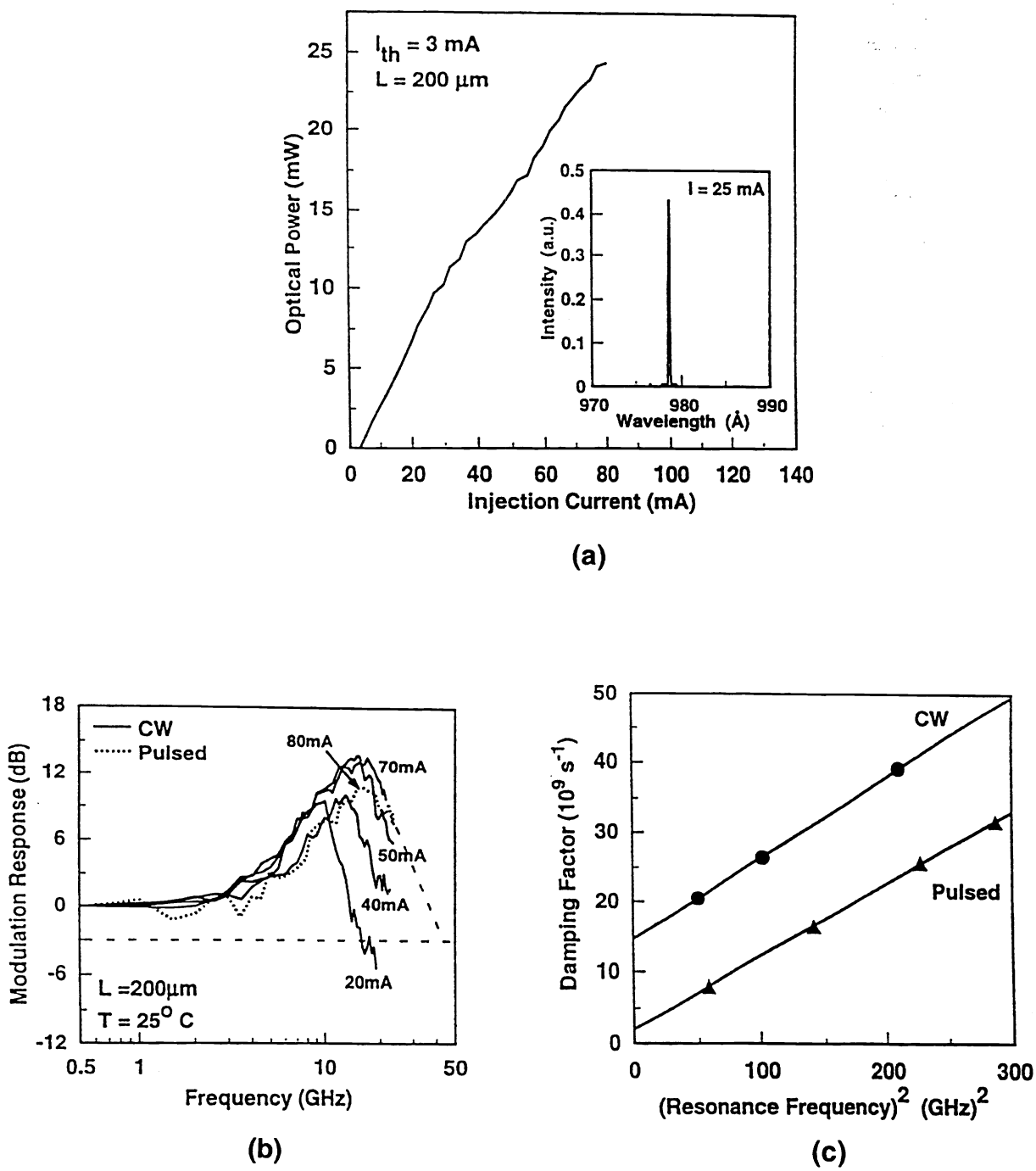

Figure 1: (a) Light-current characteristics of 4-QW 0.98 μm tunneling injection laser. The inset shows the output single mode characteristics; (b) modulation frequency response of the undoped MQW tunneling injection laser under CW and pulsed conditions; and (c) plots of damping factor versus resonance frequency squared.

It is believed that the frequency response of these lasers is limited by heating effects and with better mounting and heat-sinking higher bandwidths can be measured. It is also clear that the value of $f_{3\ dB(max)}$ may approach 100 GHz in these devices which exceeds the predicted gain-compression limited bandwidths of 60-70 GHz in high performance GaAs-based quantum well lasers. Large bandwidths can only be achieved at the expense of a very high photon density, which would definitely induce facet damage. It is therefore apparent that to achieve high modulation bandwidths, the laser has to be operated with a lower photon density, the gain compression factor ε has to be reduced and dg/dn has to be enhanced. The tunneling mechanism and "cold" operation reduce spectral hole burning and gain compression effects and increase the differential gain. Similarly, the differential gain is extracted form the relationship between resonance frequency and net injection current, I-I_{th}, and the internal conversion efficiency and optical confinement[5]. Values for internal conversion efficiency and optical confinement factor calculated at room temperature were used in the calculation at lower temperatures. The differential gain increases from ~$7x10^{-15}$ cm^2 (which is in itself a very high value) to $3x10^{-14}$ cm^2 at 120K. The gain compression factor in these devices is also very small, ~10^{-23} m^3 for pulsed or cw operation.

3. InP-BASED 1.55μm LASERS

1.55μm distributed feedback (DFB) lasers have emerged as the most promising sources for coherent communication systems. Not only have linewidths as small as 70 kHz[6] been measured in 1.55μm DFB lasers, but the ability to tune the output precisely by varying and grating period makes the devices very attractive for wavelength-division-multiplexed (WDM), fiber-optical communication systems. We have investigated the properties of 1.55μm tunneling injection DFB lasers grown by MOCVD in two steps.[7]

The active (gain) region consists of five 1% strain-compensated 80Å InGaAsP quantum wells with -1% 70Å InGaAsP barriers exhibiting a room temperature photoluminescence (PL) peak at 1.53-1.54μm. The compressively strained wells reduce intervalence band absorption, as a loss mechanism, to some extent and provide a wider optical gain spectrum.[8] The sample was first grown up to the 0.2μm InGaAsP buffer layer (λ_g=1.1μm). The DFB grating was formed by direct electron-beam writing. The grating lines were aligned along the $\langle 011 \rangle$ direction so that the ridge waveguides are along the $\langle 011 \rangle$ direction. The inner cladding layer and the quantum-well (QW) barrier regions are so chosen that the energy separation between the tunneling eigenstate and the multiquantum-well (MQW) ground states is approximately equal to the energy of an optical phonon in InP. Thus, it is envisaged that electrons are injected in this device by longitudinal optical (LO) phonon assisted tunneling. The QW sizes are so designed that the electron wavefunctions are uniformly distributed over the entire active region. The depth of the grating was approximately 800Å, to achieve a coupling constant of ~150 cm^{-1}. The sample was then prepared for MOVPE regrowth and the 1.5μm p-type InP layer, the graded layer and the $In_{0.53}Ga_{0.47}As$ p-contact layer were successively grown. A standard single-mode ridge waveguide laser was then fabricated by a combination of photolithography techniques, wet and dry etching and contact metallization. The ridge was etched to a depth of ~1.5μm from the top.

The measured temperature-dependent light versus current (L-I) characteristics for a 300μm long device was measured. The slope efficiency is only slightly lower than Fabry-Perot lasers and the output power is larger by a factor of 3.5. The temperature-dependent threshold current density is plotted in Fig. 2(a). The temperature T_o is estimated to be 120 K around room temperature and below and decreases to 70 K at higher temperatures. Again, part of this degradation is due to lack of appropriate heat sinking. Nonetheless, the measured values of T_o are significantly higher than those reported earlier for 1.55μm lasers[9, 10] and is believed to predominantly result from the tunneling injection mechanism. It is worthwhile to note that the value of T_o measured in 1.55μm Fabry-Perot tunneling injection lasers is 70 K for the temperature range 298-328 K, without any heat sinking. The value of T_o is in reasonable agreement with the value obtained for the present DFB lasers in the high temperature range (T>313 K).

Figure 2(b) shows typical responses of a 1.55μm TI laser at 290K, together with the best fit to the modulation response equation[11], The maximum measured bandwidth was about 24 GHz at room temperature. Other researchers have measured comparable values (30 GHz) at this wavelength at room temperature.[12]

4. HIGH-SPEED QUANTUM DOT LASERS

Self-organized growth of InGaAs/GaAs strained epitaxial layers gives rise to an ordered array of islands via the Stranski-Krastanow growth mode, for misfits >1.8%. These islands are pyramidal in shape with a base diagonal of ~20 nm and height of ~6-7 nm, depending on growth parameters. They therefore exhibit electronic properties of zero-dimensional systems, or quantum dots. One or more layers of such quantum dots can be stacked and vertically coupled to form the gain region of lasers. We have investigated the properties of such single-layer quantum dot (SLQD) and multilayer quantum dot

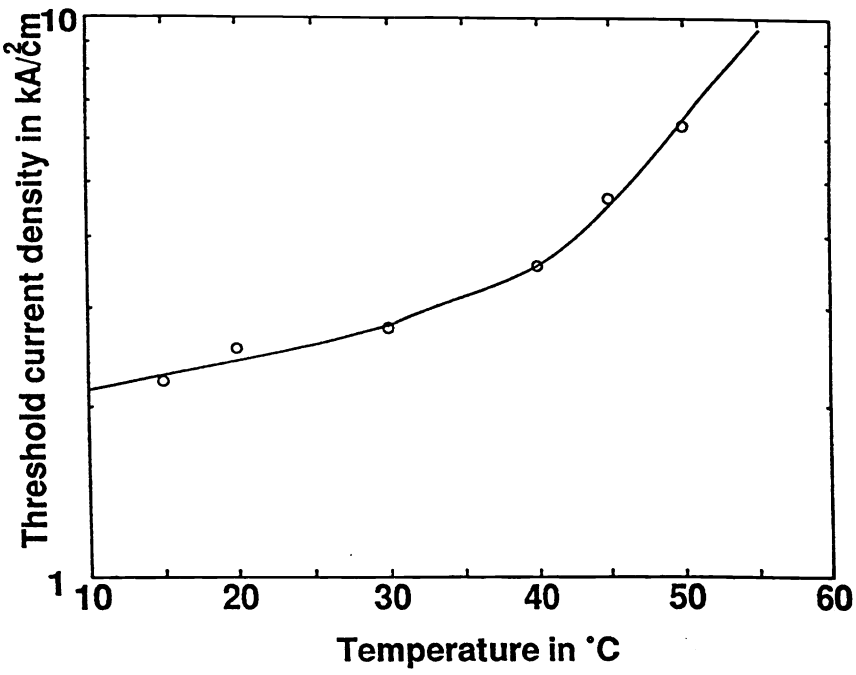

(a)

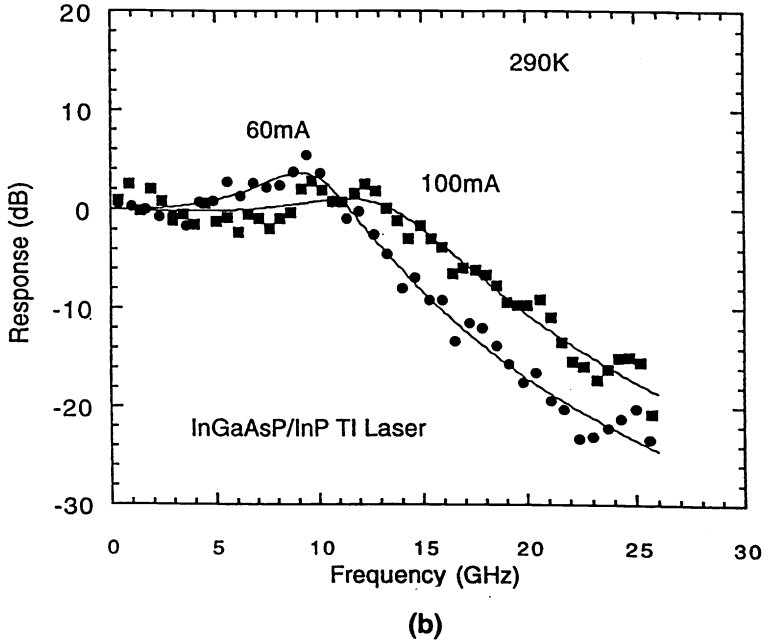

(b)

Figure 2: (a) Variation of threshold current density of 300 μm InGaAsP/InP tunneling injection DFB laser (λ=1.55 μm) with ambient temperature; (b) measured modulation response at different drive currents.

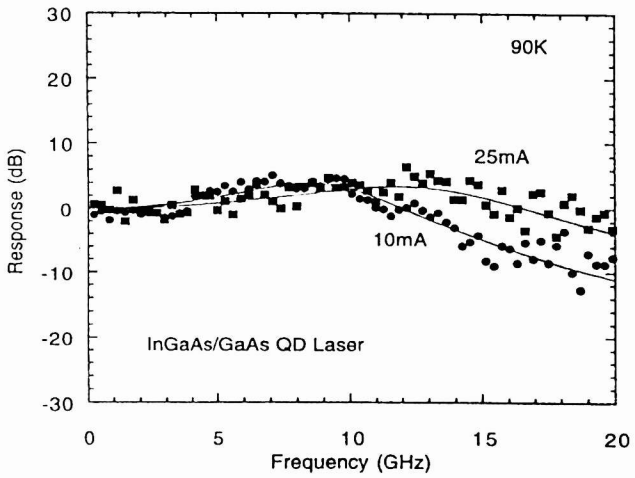

Figure 3: Small-signal modulation response of $In_{0.4}Ga_{0.6}As/GaAs$ self-organized quantum dot laser at 90K. The 3-dB bandwidth of the device is over 20 GHz.

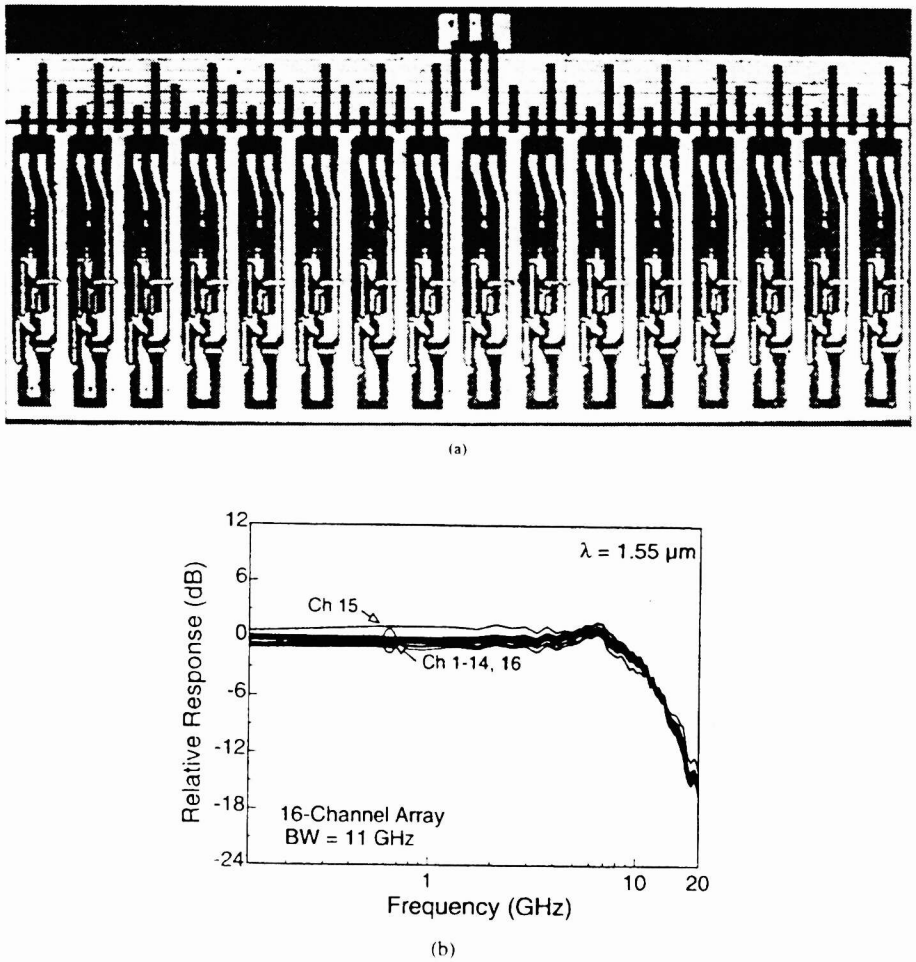

Figure 4: (a) Microphotograph and (b) frequency response of a fabricated dual-biased 16-channel array with an interchannel separation (pitch) of 250 μm.

(MLQD) lasers with a variety of measurements, including some at cryogenic temperatures. The experiments have been complemented with theoretical calculations of the electronic properties and carrier scattering phenomena in the dots. Our objective has been to elucidate the intrinsic behavior of these devices. The lasers exhibit temperature independent threshold currents up to 85 K, with $T_O \leq 670$ K. Typical threshold currents of 200μm long room temperature lasers vary from 6 to 20 mA. The small-signal modulation bandwidths of ridge waveguide lasers are 5-7.5 GHz at 300 K and increased to >20 GHz at 80 K (Fig. 3). These bandwidths agree well with electron capture times of ~30 ps determined from high-frequency laser impedance measurements at 300 K[14] and relaxation times of ~8 ps measured at 18 K by differential transmission pump-probe experiments.[15] From the calculated results we believe that electron-hole scattering intrinsically limits the high-speed performance of these devices, in spite of differential gains as high as $\sim 7 \times 10^{-14}$ cm^2 at room temperature.

5. MULTICHANNEL 1.55 μm PHOTORECEIVER ARRAYS

InP-based monolithic photoreceiver arrays with as many as eight channels have been reported.[16-18] Among them, the largest bandwidth achieved for an eight-channel array based on an InP/InGaAs *pin*/heterojunction bipolar transistor (*pin*/HBT) technology was 1.7 GHz per channel. Larger bandwidths have been reported for four-channel arrays.[19]

The monolithically integrated *pin*/HBT transimpedance-amplifier photoreceiver array was fabricated using an optimized InP/InAlAs/InGaAs HBT structure with a 6500Å-thick InGaAs precollector layer. The epitaxial heterostructure was grown by solid-source molecular beam epitaxy (SSMBE) on an Fe-doped semi-insulating InP (001) substrate and consists of a standard lattice-matched $In_{0.52}Al_{0.48}As/In_{0.53}Ga_{0.47}As$ HBT. It has a 4000Å Si-doped *n*+ (1×10^{19}cm^{-3}) InGaAs subcollector, a 6500Å *n* (1×10^{16}cm^{-3}) InGaAs collector, which is also used as the absorption region of the *pin* diode, a 750Å Be-doped *p*+ (2×10^{19}cm^{-3}) InGaAs base, a 150Å *p*-type (2×10^{18}cm^{-3}) InGaAs spacer, a 1500Å *n*-type (8×10^{17}cm^{-3}) InAlAs emitter, a 700Å *n*+ (10^{19}cm^{-3}) InAlAs layer, and a 1000Å *n*+ (10^{19}cm^{-3}) InGaAs contact layer.

The design, modeling and characterization of identical signal-channel photoreceiver circuits have been described by us in detail in[20]. The circuit topology of each photoreceiver channel includes a 156 μm^2 *pin* photodetector and a three-stage transimpedance amplifier with an output impedance matched to 50Ω. The photoreceiver arrays are centered on a 250 μm pitch. The three-stage transimpedance amplifier used in each channel of the array, which consists of 5 x 5 μm^2 HBTs and a feedback resistor of 560Ω, demonstrated a typical gain of 46dBΩ with an electrical bandwidth of 11.5 GHz. The thin-film resistors consist of 10 μm wide and a 700Å thick evaporated Ni-Cr alloy. The spiral peaking inductor was realized using Ti/Al/Ti/Au interconnection metallization of 1.5 μm total thickness. Figure 4(a) shows a microphotograph of a fabricated 16-channel *pin*/HBT photoreceiver array.

The small-signal optical frequency response of the fabricated 16-channel photoreceiver array is shown in Fig. 4(b). The array demonstrated a well-matched response in a -3dB optical-to-electrical bandwidth of 11.5±0.2 GHz and an average transimpedance gain of 46 dBΩ with a variation of <2dB. Adjacent channel crosstalk was measured by coupling the optical signal into one channel and measuring the RF output at the adjacent channels. Special care was taken to ensure that all the channels of the test array had similar gain and frequency response characteristics. Separate bias sources are used to optimize the photodiode and amplifier characteristics independently. The neighboring channel (channel 7) shows a maximum crosstalk of <-24dB. To further reduce the crosstalk, metal shields which cover the individual channels of the array[21], were fabricated by electroplating. The shield is fabricated at a height of 3 μm above the surface and covers the entire circuit except the photodiode. The metal shields block the radiated electromagnetic fields, resulting in more than 10dB reduction in crosstalk. The maximum crosstalk is measured to be <-35dB. The measured bandwidth in similar single-channel photoreceivers are 24-26 GHz. At the present time these integrated photoreceivers demonstrate the best performance in terms of bandwidth, sensitivity and crosstalk.

ACKNOWLEDGMENTS

The author acknowledges work done by A. Gutierrez-Aitken, X. Zhang, K.C. Syao, R. Bhat, C. Caneau, K. Kamath, Y. Yuan and D. Klotzkin. The work was supported by ARO and DARPA.

REFERENCES

1. T.P. Lee, et al., "Multiwavelength DFB laser array transmitters for ONTC reconfigurable optical network testbed", *IEEE J. Lightwave Tech.*, **14**, pp. 967-975, 1996.

2. S.J.B. Yoo, "Wavelength conversion technologies for WDM network applications", *IEEE J. Lightwave Tech.*, **14**, pp. 955-966, 1996.

3. C.A. Brackett, "Dense wavelength division multiplexing networks: Principles and applications", *IEEE J. Select. Areas Commun.*, **8**, p. 948, 1990.

4. J.D. Ralston, S. Weisser, E.C. Larkins, A. Schoenfelder, J. Daleiden, K. Dzotscher, M. Maier, J. Fleissner, W. Benz and J. Rosenzweig, presented at *Photonics West '96,* San Jose, California, January 27-February 2, 1996.

5. R. Nagarajan, M. Ishikawa, T. Fukushima, R.S. Geels and J.E. Bowers, "High speed quantum-well lasers and carrier transport effects", *IEEE Journ. of Quan. Electron.*, **28**, pp. 1990-2008, 1992.

6. H. Bissessur, C. Starck, J-Y. Emery, F. Pommereau, C. Duchemin, J-G. Provost, J-L. Beylat and F. Fernier, *Electron. Lett.*, **28**, pp. 998-999, 1992.

7. P. Bhattacharya, Y. Yuan, T. Brock, C. Caneau and R. Bhat, "Temperature dependence of the threshold current in 1.55-μm strain-compensated multiquantum-well distributed-feedback lasers", *IEEE Photon. Tech. Lett.*, **10**, pp. 778-780, 1998.

8. J.S. Osinski, Y. Zou, P. Grodzinski, A. Mathur and P.D. Dapkus, "Low-threshold-current-density 1.5 μm lasers using compressively strained InGaAsP quantum wells", *IEEE Photon. Technol. Lett.*, **4**, pp. 10-13, 1992.

9. C.E. Zah, P.S.D. Lin, F. Favire, B. Pathak, R. Bhat, C. Caneau, A.S. Gozdz, N.C. Andreadakis, M.A. Koza, T.P. Lee, T.C. Wu and K.Y. Lau, *Electron. Lett.*, **28**, pp. 824-826, 1992.

10. Y. Zou, J.S. Osinski, P. Grodzinski, P.D. Dapkus, W.C. Rideout, W.F. Sharfin, J. Schelafer and F.D. Crawford, "Experimental study of Auger recombination, gain, and temperature sensitivity of 1.5 μm compressively strained semiconductor lasers", *IEEE J. Quantum Electron.*, **29**, pp. 1565-1575, 1993; G.L. Belenky, R.F. Kazarinov, J. Lopata, S. Luryi, T. Tanbun-Elk and P.A. Garbinski, "Direct measurement of the carrier leakage out of the active region in InGaAsP/InP laser heterostructures", *IEEE Trans. Electron Devices,* **42**, pp. 215-218, 1995.

11. R. Nagarajan, M. Ishikawa, T. Fukushima, R. Geels, J. Bowers, "High speed quantum well lasers and carrier transport effects", *IEEE J. Quant. Electron.*, **28**, pp. 1990-2008, 1992.

12. R. Schatz, O. Kjebon, S. Lourdudoss, S. Nilsson, B. Stalnacke, "30GHz direct modulation bandwidth in detuned loaded InGaAsP DBR lasers at 1.55 μm wavelength", *Electron. Lett.*, **33**, pp. 488-489, 1997.

13. I.N. Stranski and L.V. Krastanow, *Akad. Wiss. Lett. Mainz Math. Natur.*, **146**, p. 797, 1939.

14. D. Klotzkin, K. Kamath and P. Bhattacharya, "Quantum capture times at room temperature in high-speed $In_{0.4}Ga_{0.6}As$-GaAs self-organized quantum dot lasers", *IEEE Photon. Technol. Lett.*, **9**, p. 1301, 1997.

15. T.S. Sosnowski, T.B. Norris, H. Jiang, J. Singh, K. Kamath and P. Bhattacharya, "Rapid carrier relaxation in $In_{0.4}Ga_{01.16}As$/GaAs quantum dots characterized by differential transmission spectroscopy", *Phys. Rev. B,* **57**, pp. R9423-R9426, 1998.

16. K. Aga, H. Yano, M. Murata, H. Kamel, G. Sasaki and H. Hayashi, "High-speed eight-channel optoelectronic integrated receiver arrays comprising GaInAs pin PDs and AlInAs/GaInAs HEMTs", *Tech. Dig., Opt. Fiber Comm. Conf. (OFC '91),* San Diego, CA, February 1991.

17. S. Chandrasekhar, L.D. Garrett, L.M. Lunardi, A.G. Dentai, C.A. Burrus and E.C. Burrows, "Investigation of crosstalk performance of eight-channel pin/HBT OEIC photoreceiver array modules", *IEEE Photonics Technol. Lett.*, **8**, pp. 682-684, 1996.

18. W.S. Lee, D.A.H. Spear, A.D. Smith, S.A. Wheeler and S.W. Bland, "Monolithic eight-channel photoreceiver array OEICs for HDWDM applications at 1.55 μm", *Electron. Lett.*, **28**, pp. 612-614, 1992.

19. H. Yano, G. Sasaki, N. Nishiyana, M. Murata, H. Kamiyama and H. Hayashi, "5Gbit/s four-channel receiver optoelectronic integrated circuit array for long-wavelength lightwave systems", *Electron. Lett.*, **28**, pp. 503-504, 1992.

20. K. Yang, A.L. Gutierrez-Aitken, X. Zhang, G.I. Haddad and P. Bhattacharya, "Design, modeling, and characterization of monolithically integrated InP-based (1.55 μm) high-speed (24GB/s) p-i-n/HBT front-end photoreceivers", *J. Lightwave Technol.*, **14**, pp. 1831-1839, 1996.

21. A.L. Gutierrez-Aitken, P. Bhattacharya, K.C. Syao, K. Yang, G.I. Haddad and X. Zhang, "Low crosstalk (<-40dB) in 1.55 μm high speed OEIC photoreceiver arrays with novel on-chip shielding", *Electron. Lett.*, **32**, pp. 1706-1708, 1996.